Cellular/Molecular

Ca^{2+}/Calmodulin Regulates Trafficking of $Ca_V1.2$ Ca^{2+} Channels in Cultured Hippocampal Neurons

Hong-Gang Wang,[1]* Meena S. George,[3]* James Kim,[1] Chaojian Wang,[1] and Geoffrey S. Pitt[1,2]

Departments of [1]Pharmacology and [2]Medicine, Division of Cardiology, [3]Center for Neurobiology and Behavior, College of Physicians and Surgeons of Columbia University, New York, New York 10032

As the Ca^{2+}-sensor for Ca^{2+}-dependent inactivation, calmodulin (CaM) has been proposed, but never definitively demonstrated, to be a constitutive $Ca_V1.2$ Ca^{2+} channel subunit. Here we show that CaM is associated with the $Ca_V1.2$ pore-forming α_{1C} subunit in brain in a Ca^{2+}-independent manner. Within its CaM binding pocket, α_{1C} has been proposed to contain a membrane targeting domain. Because ion channel subunits assemble early during channel biosynthesis, we postulated that this association with CaM could afford the opportunity for Ca^{2+}-dependent regulation of membrane targeting. We showed that the isolated domain functioned as a Ca^{2+}/CaM regulated trafficking determinant for CD8 (a model transmembrane protein) using fluorescent-activated cell sorting analysis and, using green fluorescent protein-tagged α_{1C} subunits expressed in cultured hippocampal neurons, that Ca^{2+}/CaM interaction with this domain accelerated trafficking of $Ca_V1.2$ channels to distal regions of the dendritic arbor. Furthermore, this Ca^{2+}/CaM-accelerated trafficking was activity dependent. Thus, CaM imparts Ca^{2+}-dependent regulation not only to mature $Ca_V1.2$ channels at the cell surface but also to steps during channel biosynthesis.

Key words: **calcium; calcium channels; calmodulin; channel; hippocampus; trafficking**

Introduction

Neuronal responses to electrical activity, such as neurotransmitter release or long-term potentiation, result from changes in intracellular Ca^{2+}, which modulates a multitude of Ca^{2+} binding proteins (CaBPs) with distinct but overlapping effectors. Because ion channels are among these effectors, Ca^{2+} can provide feedback regulation to the very proteins that regulate membrane excitability. Most extensively studied is Ca^{2+}-dependent inactivation (CDI) of L-type $Ca_V1.2$ Ca^{2+} channels (Budde et al., 2002).

The CDI sensor is thought to be calmodulin (CaM), the prototypical CaBP. CaM controls CDI through interaction with a ~110 aa binding pocket in the C terminus (CT) of α_{1C} in which one critical determinant is a consensus CaM binding "IQ" motif (Peterson et al., 1999; Zühlke et al., 1999). Other sites in the binding pocket are also essential, and mutations throughout the binding pocket that disrupt CaM interaction occlude the expression of CDI (Kim et al., 2004). Based on biochemical, imaging, and functional analyses, CaM has been predicted (but never definitively demonstrated) to be an obligate $Ca_V1.2$ subunit, bound to α_{1C} in basal levels of $[Ca^{2+}]_i$ and poised to trigger CDI when $[Ca^{2+}]_i$ increases (Pitt et al., 2001).

Because ion channel subunits associate early during channel biosynthesis (Deutsch, 2003), we hypothesized that CaM could also affect diverse processes during channel biosynthesis in addition to regulating CDI. Thus, it was particularly intriguing that the α_{1C} CT contains a domain within the CaM binding pocket that is necessary for proper plasma membrane targeting of $Ca_V1.2$ channels (Gao et al., 2000). Because $Ca_V1.2$ channels are central to cAMP response element-binding protein (CREB)-dependent gene expression paradigms in the hippocampus that underlie learning and memory and specific targeting of $Ca_V1.2$ channels is necessary for CREB-dependent gene expression (Deisseroth et al., 2003; Weick et al., 2003), we postulated that Ca^{2+}/CaM may regulate $Ca_V1.2$ trafficking in hippocampal neurons, thereby contributing to activity-dependent gene expression paradigms.

Materials and Methods

Molecular biology. The green fluorescent protein (GFP)–α_{1C} construct was constructed as described previously (Grabner et al., 1998). The GFP–α_{1C}–CaM and GFP–α_{1C}–CaM_{1234} concatemers with a 12× glycine linker between the truncated α_{1C} (at amino acid 1669) and CaM or CaM_{1234} were generated following the general strategy as outlined previously (Mori et al., 2004). The myc–CD8–Ca^{2+} in activation region peptide (CIRP) constructs were generated by standard molecular biology techniques. The construct consists of an extracellular myc tag linked to the extracellular and transmembrane domains of CD8α (amino acids 1–206) linked to the CIRP region of α_{1C} (amino acids 1507–1669).

Fluorescent-activated cell sorting. Human embryonic kidney 293T (HEK293T) cells were maintained in 5% CO_2 at 37°C in DMEM supplemented with 10% FBS, L-glutamine, penicillin, and streptomycin. Cells

Received Dec. 30, 2006; revised July 9, 2007; accepted July 9, 2007.

This work was supported by National Institutes of Health Grant HL 71165 and American Heart Association Grant 0555875T (both to G.S.P.). G.S.P. is a recipient of the Irma T. Hirschl Career Scientist Award and is the Esther Aboodi Assistant Professor of Medicine. M.S.G. is supported by the Medical Scientist Training Program. We thank Leonard Zablow for technical assistance. We also thank members of the Alexandropoulos laboratory for advice, help, and reagents for FACS analysis.

*H.-G.W. and M.S.G. contributed equally to this work.

Correspondence should be addressed to Geoffrey S. Pitt, Department of Medicine, Duke University Medical Center, Durham, NC 27710. E-mail: geoffrey.pitt@duke.edu.

DOI:10.1523/JNEUROSCI.1720-07.2007

 0270-6474/07/279086-08$15.00/0

were transfected using calcium phosphate (Chemicon, Temecula, CA). In brief, 11–21 μg of DNA *in toto* were used to transfect cells grown to a ~60% density on a 6 cm dish. The DNA ratio of GFP to myc–CD8–CIRP was 1:10. When CaM or CaM_{1234} was cotransfected with myc–CD8–CIRP, the DNA ratio of CaM to myc–CD8–CIRP was 1:1. Cells were harvested ~40 h after transfection and surface stained with an anti-myc antibody conjugated to the fluorophore PBXL-3 (Martek, Columbia, MD). Staining was performed following a standard fluorescent-activated cell sorting (FACS) staining protocol with at least 45 min of incubation with a 1:100 dilution of the antibody. The FACS wash used during spins and staining contained 1% BSA and 0.1% sodium azide in PBS. Cells were fixed with 4% paraformaldehyde in PBS. Samples were analyzed on a BD LSRII at the Columbia University Flow Cytometry Facility. A total of 30,000 cells were collected for each sample for each of three trials. The LSRII uses BD FACS DiVa software. Data analysis was performed using Flow-Jo (version 8.1.0), and statistical comparisons were done using Student's *t* test.

HEK293 cell culture and transfection for electrophysiology and confocal imaging. HEK293 cells were maintained in 5% CO_2 at 37°C in DMEM supplemented with 10% FBS, L-glutamine, penicillin, and streptomycin. A stable cell line expressing the calcium channel auxiliary subunits β_1 and $\alpha_2\delta$ was maintained as above with the addition of G418 (500 μg/ml). Cells were transfected using $CaCl_2$. In brief, 5–10 μg of DNA *in toto* were used to transfect cells grown to a ~25% density on a 10 cm dish. When GFP was used to visualize transfected cells, the DNA ratio of GFP to α_{1C} was 1:10. When CaM or CaM_{1234} was cotransfected with α_{1C}, the DNA ratio of CaM or CaM_{1234} to α_{1C} was 10:1, increasing the likelihood that cells transfected with α_{1C} also contained transfected CaM or CaM_{1234}.

Electrophysiological recordings were performed 2 d after transfection. Whole-cell patch-clamp currents recorded from HEK293 cells were obtained with an Axopatch 200B amplifier. The internal pipette solution contained the following (in mM):190 *N*-methyl-D-glucamine (NMG), 5 EGTA, 4 $MgCl_2$, 40 HEPES, pH 7.25, and 2 ATP, supplemented with 12 μM phosphocreatine. The external solution contained the following (in mM): 130 NMG-aspartate, 1 $MgCl_2$, 10 glucose, 10 4-aminopyridine, 10 HEPES, pH 7.4, and 10 $BaCl_2$. Series resistance was compensated by 70%. Currents were sampled at 10 kHz and filtered at 2 kHz. Gating currents were obtained by depolarizations to the reversal potential. Data are presented as mean ± SEM.

For confocal imaging, HEK cells grown on coverslips were rinsed with PBS, fixed with ice-cold methanol, and mounted in Citifluor. Images were obtained on a Zeiss (Oberkochen, Germany) LSM 510 confocal microscope at the Columbia University Health Sciences Optical Microcopy Facility.

Neuronal cultures and imaging. Hippocampi from 1–2 d newborn rats (Sprague Dawley strain) were dissociated through enzymatic treatment with 0.25% trypsin and subsequent trituration. The cells were plated on glass coverslips previously coated with poly-D-lysine. Hippocampal cells were grown in neurobasal A medium (Invitrogen, Carlsbad, CA) supplemented with 2% B27, 2 mM glutamine, and 10% heat-inactivated bovine calf serum. After 24 h, this medium was replaced by one containing 0.5 mM glutamine, 1% heat-inactivated bovine calf serum, 0.5 mM kynurenic acid, 70 μM uridine, and 25 μM 5-fluorodeoxyuridine. Hippocampal neurons grown for 6–7 d in culture were transfected with the indicated plasmids using calcium phosphate precipitation, as described previously (Deisseroth et al., 1998). Some neurons were cotransfected with red fluorescent protein (RFP) (pDsRed2; Clontech, Mountain View, CA). Fluorescent images in live cells were obtained at 1, 3, 5, and 14 d after transfection. When testing the activity dependence of trafficking, cells were made quiescent 6 h after transfection by incubation for 60 min in Tyrode's solution containing (in mM) 119 NaCl, 3 KCl, 20 HEPES, 2 $CaCl_2$, 2 $MgCl_2$, 30 glucose, and 1 μM TTX, pH 7.3, and then stimulated with hyperkalemic solution containing the following (in mM): 77 NaCl, 45 KCl, 20 HEPES, 2 $CaCl_2$, 2 $MgCl_2$, and 30 glucose, pH 7.3 for 3 min. All images were acquired using a Bio-Rad (Hercules, CA) MRC 1000 confocal laser scanning system coupled to a Zeiss Axiovert 100 inverted microscope. For each image acquisition, a Kalman average of five frames was used. Trafficking was quantified by measuring the longest fluorescent dendritic branch with NIH ImageJ 1.35p, and data were analyzed with the Kolmogorov–Smirnov test.

CaM coimmunoprecipitation and immunoblots. Adult rat brain was washed twice with ice-cold PBS and homogenized with glass homogenizer 20 times in 4 vol of ice-cold PBS with protease inhibitor cocktail (Roche, Indianapolis, IN). The homogenate was centrifuged at 16,000 × *g* at 4°C for 20 min. The pellet was resuspended in 150 mM NaCl, 50 mM Tris, pH 7.5, 10 μM $CaCl_2$ (buffer A) plus protease inhibitors and 1% Triton X-100 and incubated for 1 h at 4°C and then recentrifuged. Protein (1.8 mg) was incubated in buffer A plus 0.25% Triton X-100 and free Ca^{2+} as indicated (Ca^{2+} buffering was performed with 5 mM BAPTA using calculations derived from WEBMAXC STANDARD, http://www.stanford.edu/~cpatton/maxc.html). Anti-α_{1C} (Alomone Labs, Jerusalem, Israel) was added to the samples, which were incubated for 1 h at 4°C, and then overnight at 4°C with protein A plus G beads. Samples were washed with buffer A plus 0.25% Triton X-100 supplemented with free Ca^{2+} as indicated and protein (10 μg) was loaded on SDS-PAGE gels. For anti-α_{1C} immunoblot, protein was transferred to nitrocellulose. For anti-CaM immunoblot, protein was transferred to polyvinylidene difluoride at 4°C for 16 h in 50 mM potassium phosphate, pH 7.0, and fixed to the membrane by incubation with freshly prepared glutaraldehyde (0.2% in the phosphate buffer) for 20 min. EGTA (1 mM) was added to all samples before SDS-PAGE. Immunoblots were performed with anti-CaM antibody (Upstate Biotechnology, Lake Placid, NY).

For GFP immunoblots, HEK293 cells were washed with ice-cold TBS (150 mM NaCl and 50 mM Tris, pH 7.5), harvested, and resuspended in ice-cold TBS with 1% Triton X-100 and protease inhibitor 2 d after the cells had been transfected with the respective plasmids. Cells were lysed by pipetting up and down and then centrifuged at 16,000 × *g* for 20 min. Protein was then separated by SDS-PAGE, transferred to nitrocellulose, and immunoblotted with anti-GFP antibody (Covance, Princeton, NJ).

Results

CaM is constitutively associated with $Ca_V1.2$ channels in brain

To test whether CaM is constitutively associated with $Ca_V1.2$ in tissue, we checked whether CaM coimmunoprecipitated with α_{1C} from rat brain lysates. As shown in Figure 1*A*, CaM was detected in α_{1C} immunoprecipitates when elevated Ca^{2+} (10 μM) or nominal basal Ca^{2+} (100 nM) was added to the buffer. These results suggested that CaM functions as a true channel subunit and remains associated with $Ca_V1.2$ channels at basal levels of Ca^{2+}.

CaM controls activity-dependent trafficking of $Ca_v1.2$ channels in hippocampal neurons

The previous identification of a plasma membrane targeting sequence (amino acids 1623–1666) within the CaM binding pocket of α_{1C} (Gao et al., 2000), and the constitutive nature of the interaction between CaM and α_{1C} led us to investigate whether CaM regulated α_{1C} trafficking in hippocampal neurons. In this role, CaM could allow Ca^{2+}-dependent trafficking of α_{1C} that was responsive to activity. To assess trafficking, we expressed a GFP-tagged version of α_{1C} in cultured hippocampal neurons. The addition of GFP to the α_{1C} N terminus does not alter any functional properties of $Ca_V1.2$ channels (Grabner et al., 1998) and was thus a convenient tool for visualizing the subcellular distribution of channels. GFP–α_{1C} showed intense signal in the soma and prominent fluorescence throughout the dendritic arbor (Fig. 1*C*), consistent with the pattern observed previously in hippocampal neurons after transfection of GFP–α_{1C} or immunocytochemistry of endogenous α_{1C} (Obermair et al., 2004). Immunoblots of GFP–α_{1C} expressed in HEK cells confirmed that the fluorescent signal represented GFP–α_{1C} and not cleaved GFP (Fig. 1*B*). To assess trafficking of $Ca_V1.2$, we first devised a metric in which we measured the distance from the soma to the farthest GFP fluorescent point in the longest dendrite in each neuron and plotted these

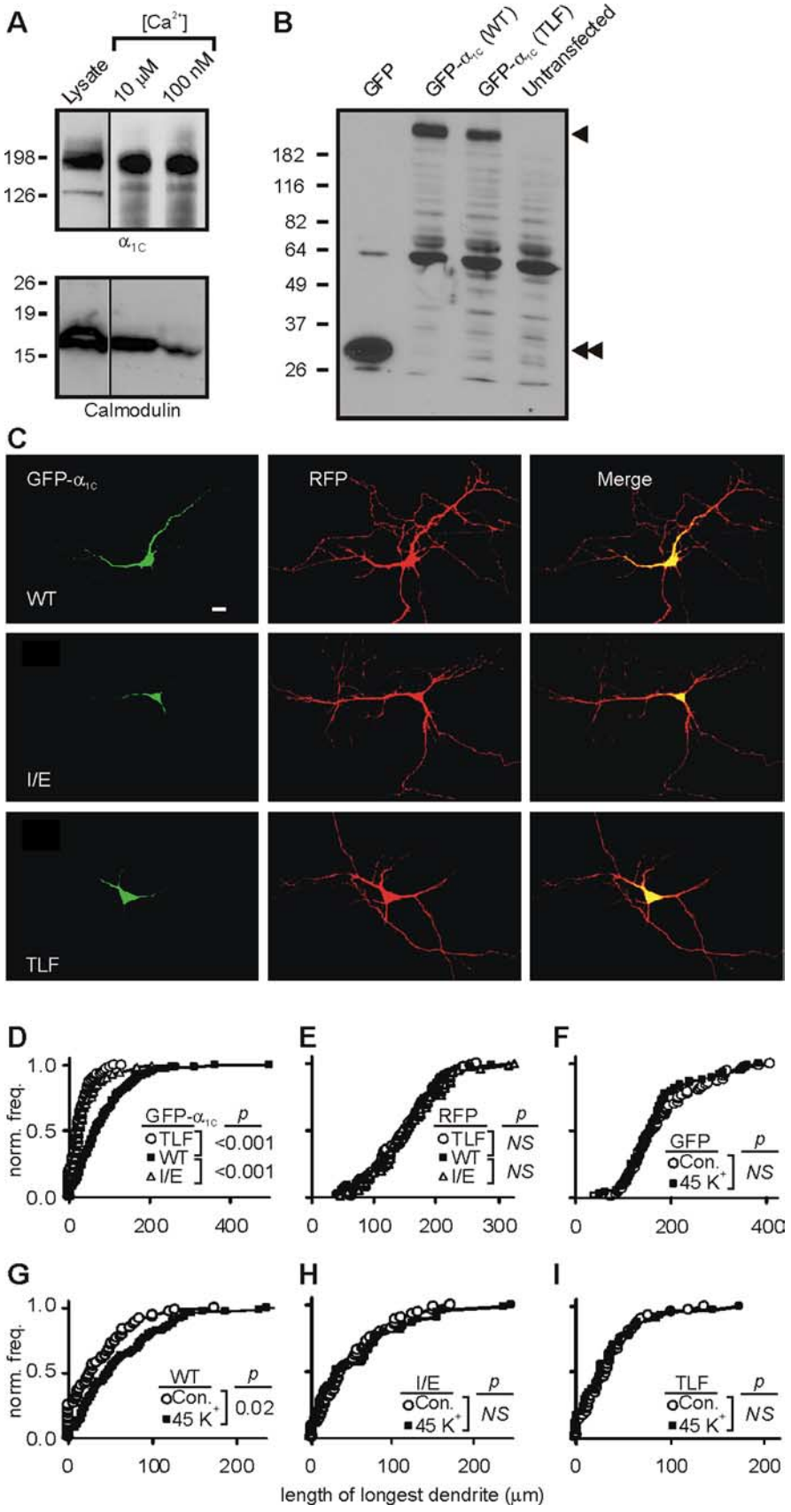

Figure 1. Constitutive association of CaM with α_{1C} in brain promotes activity-dependent $Ca_v1.2$ trafficking. ***A***, Immunoblot for α_{1C} (top) and CaM (bottom) after immunoprecipitation of α_{1C} in the presence of 10 μM Ca^{2+} or 100 nM Ca^{2+}. IgG controls were performed and did not show α_{1C} immunoprecipitation (data not shown). ***B***, Immunoblot for GFP of lysates of untransfected HEK cells or cells transfected with GFP, GFP–α_{1C}, or GFP–α_{1C} (TLF). Single arrowhead, GFP–α_{1C}; double arrowhead, GFP. ***C***, Fluorescent confocal images of hippocampal neurons transfected with RFP and cotransfected with GFP–α_{1C}, GFP–α_{1C} (I/E), or GFP–α_{1C} (TLF). Scale bar, 20 μm. ***D***, Normalized frequency versus distance from soma of GFP in the longest dendrite for each neuron for GFP–α_{1C} ($n = 193$), GFP–α_{1C} (TLF) ($n = 108$), and GFP–α_{1C} (I/E) ($n = 55$) in cultures imaged 3 d after transfection. ***E***, Normalized frequency versus distance from soma of RFP in the longest dendrite for each neuron for GFP–α_{1C} ($n = 63$), GFP–α_{1C} (TLF) ($n = 64$), and GFP–α_{1C} (I/E) ($n = 55$). ***F***, Normalized frequency versus distance from soma of GFP in the longest dendrite for each neuron stimulated with 45 mM K^+ for 3 min at 6 h after transfection ($n = 69$) versus GFP without stimulation (control, $n = 70$) and imaged 24 h after stimulation. ***G***, Same as in ***F***, but for GFP–α_{1C} ($n = 115$, stimulated; $n = 55$, control). ***H***, Same as in ***F***, but for GFP–α_{1C} (I/E) ($n = 53$, stimulated; $n = 52$, control). ***I***, Same as in ***F***, but for GFP–α_{1C} (TLF) ($n = 41$, stimulated; $n = 41$, control).

data as a normalized (to the number of neurons in each dataset) frequency distribution. We compared the normalized frequency distributions for a wild-type (WT) α_{1C}, an α_{1C} with ^{1591}TLF^{1593} mutated to AAA (TLF), and an α_{1C} with I1654E (Fig. 1*C*). We had shown previously that both mutations, I/E in the IQ motif (I/E) and TLF in a separate region of the CaM binding pocket, disrupt CaM interaction with the α_{1C} C terminus (Kim et al., 2004). As shown in Figure 1*D*, the CaM disrupting mutations significantly reduced α_{1C} trafficking assessed 3 d after transfection. This was not attributable to a mutant-induced decrease in dendritic length because cotransfection of RFP in a subpopulation of these cells showed that dendritic length was unaltered (Fig. 1*E*), nor was it attributable to a decrease in mutant protein expression because the TLF mutant was expressed at similar levels to WT GFP–α_{1C}, as shown in Figure 1*B*.

The potential role for CaM in trafficking of α_{1C} prompted us to test whether this process was sensitive to neuronal activity and the consequent Ca^{2+} influx that could activate CaM. We therefore compared trafficking in neurons depolarized with 45 mM K^+ for 3 min with neurons held quiescent. There was no activity-dependent change in distribution of GFP transfected as a control (Fig. 1*F*). However, when we compared GFP–α_{1C} trafficking, we found that activity facilitated trafficking (Fig. 1*G*). The TLF and I/E mutations, in contrast, prevented activity-dependent facilitation of trafficking (Fig. 1*H*,*I*). Together, these data suggest that Ca^{2+}/CaM may provide dynamic, activity-dependent trafficking to $Ca_v1.2$ channels.

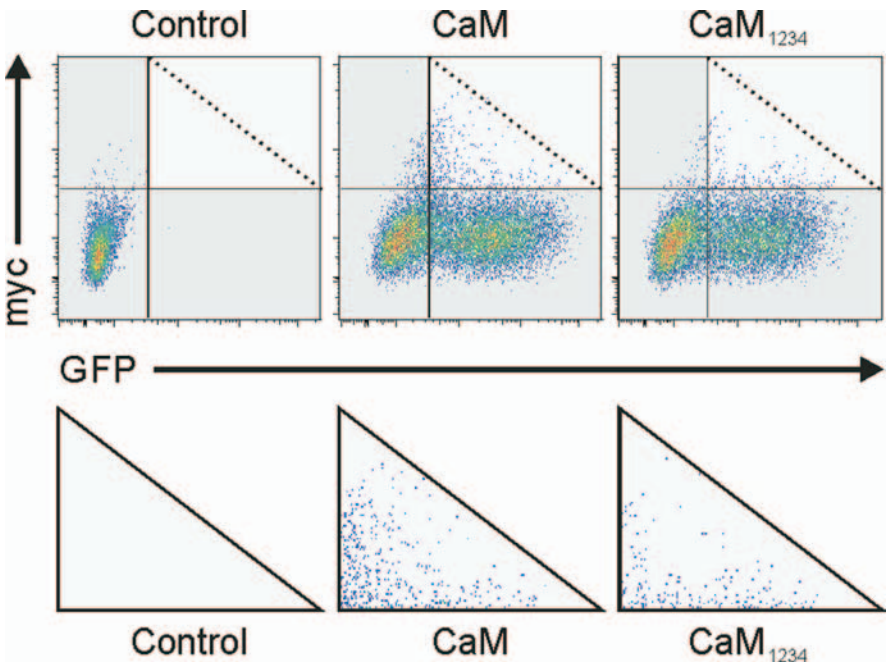

Figure 2. The CIRP region of α_{1C} contains a forward-trafficking domain regulated by Ca^{2+}/CaM. FACS analysis of HEK293 cells cotransfected with GFP, myc–CD8–CIRP, and either CaM or CaM_{1234} and stained with an anti-myc antibody. Surface staining for control untransfected cells (left), myc–CD8–CIRP plus CaM transfected cells (middle), and myc–CD8–CIRP plus CaM_{1234} transfected cells (right). Double-positive cells present in top right quadrant are shown magnified below.

The CaM binding pocket contains a Ca^{2+}/CaM-sensitive membrane targeting domain

To determine whether the previously identified membrane targeting sequence in α_{1C} (amino acids 1623–1666) contributed to Ca^{2+}/CaM trafficking of $Ca_V1.2$ channels in hippocampal neurons, we first tested whether this isolated sequence supported Ca^{2+}/CaM-dependent targeting of the unrelated, type I transmembrane protein CD8α, which is known to be constitutively trafficked to the plasma membrane (Iodice et al., 2001). We fused the CaM binding pocket of α_{1C} (CIRP, amino acids 1507–1669) to the C terminus of a myc-tagged CD8α (myc–CD8–CIRP) and assessed whether Ca^{2+}/CaM promoted its surface expression in HEK293 cells by comparing the effects of CaM versus CaM_{1234}, a mutated CaM unable to bind Ca^{2+}. The myc–CD8–CIRP was coexpressed with CaM or CaM_{1234}, and surface expression was analyzed in nonpermeabilized cells by FACS. In these experiments, GFP was cotransfected to assess the success of transfection. As can be seen in Figure 2, no GFP signal or myc–CD8 surface labeling was detected in untransfected cells. In the absence of CaM or CaM_{1234} expression, ~5% of the cells demonstrated surface expression of the myc-tagged construct; similar levels were obtained with CaM coexpression, suggesting that endogenous CaM was not limiting. In comparison, coexpression of CaM_{1234} reduced myc–CD8–CIRP surface labeling by 56 ± 6% ($n = 3$ transfections; $p = 0.02$), revealing that coexpression of CaM promotes significantly higher membrane targeting. These results indicate that CIRP may contain a retention motif that is masked by Ca^{2+}/CaM. The presence of myc–CD8–CIRP surface labeling in cells cotransfected with CaM_{1234} could reflect either that Ca^{2+}-free CaM is able to promote membrane targeting, albeit less effectively than Ca^{2+}/CaM, and/or that the coexpressed CaM_{1234} did not completely preclude the actions of endogenous CaM.

Ca^{2+}/CaM regulates membrane targeting of $Ca_V1.2$ channels

We next tested whether membrane targeting of α_{1C} in HEK cells was affected by mutations that disrupted CaM binding. We measured the resultant currents of two different $Ca_V1.2$ channels containing CaM binding mutations in α_{1C} (I/E and TLF as in Fig. 1) and currents from channels containing WT α_{1C}. As shown in Figure 3, *A* and *B*, current amplitudes from both the I/E and the TLF mutants were decreased compared with WT α_{1C}. To correlate whether this effect could be attributed to effects on trafficking/targeting, we used the GFP-labeled α_{1C} and analyzed the fluorescent distribution for the WT and mutant channels. The GFP fluorescence pattern in cells expressing TLF or I/E was different from the pattern in cells expressing WT α_{1C}. Rather than the plasma membrane-like pattern observed in cells expressing WT α_{1C}, the pattern in cells expressing the mutant channels was more clustered toward the center of the cell in an endoplasmic reticulum-like pattern (Fig. 3*C*). We also measured gating charge (Q_{ON}) during voltage steps to the reversal potential (E_{rev}) to obtain a quantitative correlate of the number of functional channels at the cell surface. The decrease in Q_{ON} for channels containing the CaM binding mutations suggested that there were significantly less functional channels at the plasma membrane than for the WT α_{1C} (Fig. 3*D*).

To confirm that these effects were attributable to CaM interaction with CIRP and to test the Ca^{2+} dependence of CaM-mediated trafficking, we compared the effects of CaM versus CaM_{1234}. In an attempt to achieve effective competition between CaM_{1234} and endogenous CaM, we truncated α_{1C} after the IQ motif at amino acid 1669 and fused CaM_{1234} (or CaM as a control) via a flexible 12 glycine linker, thereby providing a high local concentration of the mutant CaM. This general strategy, originally developed to assess the contribution of CaM to CDI, does not affect the resultant Ca^{2+} currents (Mori et al., 2004). An added advantage is that this approach restricts the actions of CaM_{1234} to α_{1C}, limiting possible nonspecific effects on the myriad CaM-related pathways that could contribute to protein trafficking. In our α_{1C}–CaM concatemers, we included GFP at the N terminus as shown in Figure 4*A* to correlate a quantitative assessment of channels at the plasma membrane (using electrophysiological recordings) with images showing the subcellular localization of the concatemers. Confocal images in Figure 4*B* of cells expressing the concatemers with CaM (GFP–α_{1C}–CaM) showed a fluorescence pattern consistent with trafficking of the channels to the membrane and similar to GFP–α_{1C} (Fig. 4*B*). In contrast, the predominant fluorescence in cells expressing concatemers with CaM_{1234} (GFP–α_{1C}–CaM_{1234}) was excluded from the cell periphery and was instead in a perinuclear distribution (Fig. 4*B*), suggesting that less channels trafficked to the plasma membrane. Peak currents recorded from these cells were markedly reduced compared with cells expressing GFP–α_{1C}–CaM (Fig. 4*C*). Q_{ON} during voltage steps to the E_{rev}, normalized for cell capacitance because the cells expressing GFP–α_{1C}–CaM_{1234} tended to be sig-

nificantly larger than the cells expressing GFP–α_{1C}–CaM, suggested that the linked CaM concatemers yielded significantly more functional channels at the plasma membrane than the linked CaM_{1234} concatemers (4.4 ± 0.7 vs 0.4 ± 0.3 mC/F; n = 5 each; p = 0.001). Thus, these data suggested that Ca^{2+}/CaM is a potent stimulator for channel trafficking through its interaction with the targeting domain in α_{1C}.

As a control for the linked CaM strategy, we also assessed the trafficking/membrane targeting of α_{1C} when CaM or CaM_{1234} was coexpressed separately. As seen in Figure 4*D*, coexpression of CaM generated significantly higher current density than coexpression of CaM_{1234}. Gating charge measurements were also higher (5.6 ± 0.4 mC/F for coexpressed CaM vs 2.5 ± 0.8 mC/F for CaM_{1234}; n = 5 each; P = 0.007) than coexpression of CaM_{1234}. Thus, the CaM-mediated trafficking of α_{1C} was Ca^{2+} dependent. Compared with the CaM_{1234}-linked constructs (Fig. 4*C*), the effects with unlinked CaM_{1234} were diminished. This incomplete inhibition was similar to what we observed for the CD8–CIRP experiments (Fig. 2), suggesting that endogenous CaM was able to compete with coexpressed unlinked CaM_{1234} and at least partially reverse the effects.

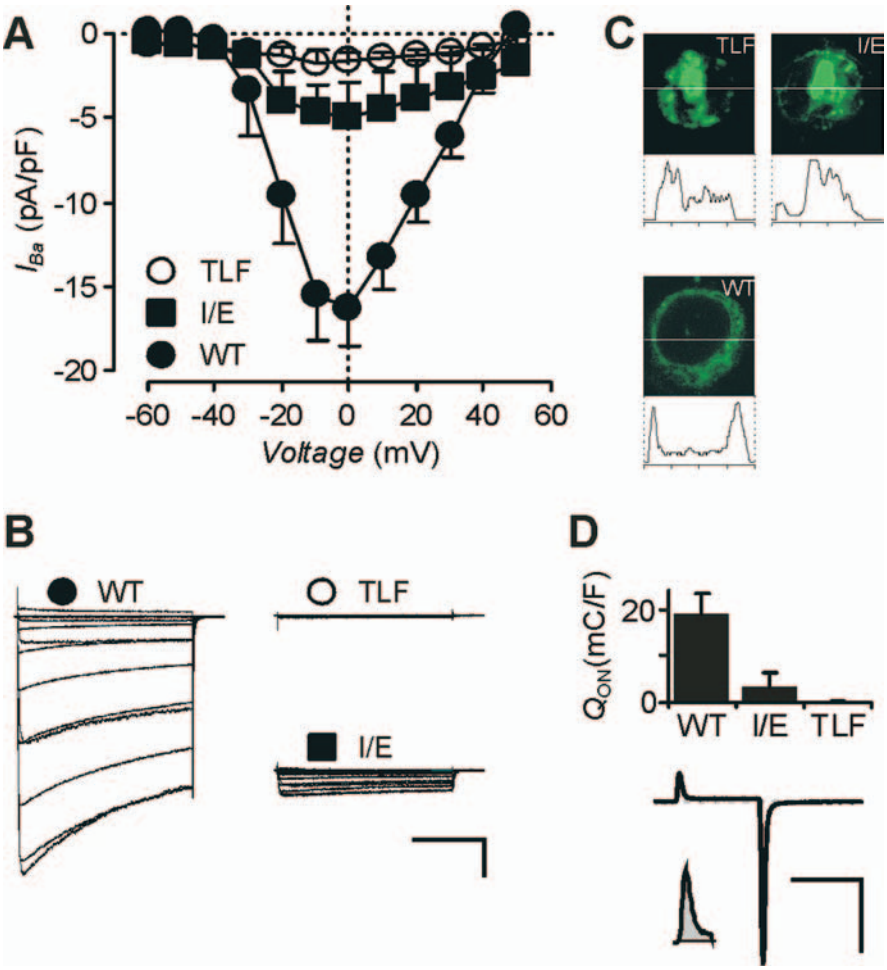

Figure 3. Mutations in the CaM binding domain of α_{1C} affect channel targeting. ***A***, Mutation of amino acids ^{1591}TLF^{1593} to alanines (TLF) or mutation of I1654E (I/E) reduced current amplitude in HEK293 cells as shown by normalized *I–V* relationships of I_{Ba} (n = 5–7). ***B***, Exemplar whole-cell I_{Ba} currents. Calibration: 200 pA, 200 ms. ***C***, Representative confocal images of GFP-tagged α_{1C} WT, TLF, and I/E and accompanying line scans showing altered cellular localization of the CaM binding mutants. ***D***, Summary of ON gating current amplitude (n = 10–14) elicited by stepping to the reversal potential (E_{rev} of approximately +55 mV). Exemplar current from a cell expressing the WT channel evoked by a 20 ms test pulse to +55 mV from V_h of −90 mV (Calibration: 2 nA, 20 ms), and a 250% magnification of the gating current is shown below.

Ca^{2+}/CaM control $Ca_V1.2$ channel trafficking in hippocampal neurons

Because Ca^{2+}/CaM interaction with the CIRP in α_{1C} appeared to mediate trafficking of α_{1C} in HEK cells, we next tested whether Ca^{2+}/CaM was responsible for the trafficking of α_{1C} in hippocampal neurons. Our general strategy was to compare the distribution of GFP–α_{1C}–CaM and GFP–α_{1C}–CaM_{1234} after transfection into cultured neurons using a similar method of analysis as in Figure 1*D*. Before proceeding with those experiments, we first analyzed whether either the addition of CaM to the α_{1C} C terminus or the truncation of α_{1C} after the IQ motif affected the distribution of α_{1C} in hippocampal neurons. This concern was motivated by previous reports showing that the distal C terminus of α_{1C} is important for localizing $Ca_V1.2$ with the machinery necessary to support CREB-dependent gene expression (Dolmetsch et al., 2001; Weick et al., 2003). When we compared the distribution of GFP–α_{1C}–CaM with GFP–α_{1C}, we found that their distributions were similar, both showing intense signal in the soma and prominent fluorescence throughout the dendritic arbor (compare Fig. 5*A* with 1*C*). Moreover, measurement of the distance from the soma to the farthest GFP fluorescent point in the longest dendrite for each neuron revealed no difference between GFP–α_{1C}–CaM and GFP–α_{1C} (Fig. 5*B*, data for 3 d after transfection). Thus, the distal end of α_{1C} is not critical for α_{1C} trafficking to distal regions of dendrites.

We therefore performed measurements with GFP–α_{1C}–CaM and GFP–α_{1C}–CaM_{1234} at several time points after transfection over a 14 d period (Fig. 5*C*). For the first 3 d after transfection, the GFP–α_{1C}–CaM trafficked farther from the soma than the CaM_{1234}-linked construct; by 5 d after transfection, the normalized frequency distributions were indistinguishable. That the CaM_{1234}-linked construct was not retained within the soma, as might be expected from the distribution of this construct when expressed in HEK cells, likely reflects the specific manifestation of Ca^{2+}/CaM-mediated effects on channel trafficking/targeting in polarized neurons compared with nonpolarized HEK cells. Additionally, we postulated that endogenous CaM might be able to compete more effectively with CaM_{1234} in these neuronal experiments because of the longer time frame. To test this hypothesis, we analyzed the time dependence of trafficking of GFP–α_{1C} (TLF) compared with GFP-α_{1C} (WT) over 14 d, because the mutation should prevent endogenous CaM interaction. As seen in Figure 5*D*, the WT channel maintained its advantage over TLF throughout the 14 d period.

Discussion

Underlying the formation of memory are certain well characterized types of synaptic plasticity that require Ca^{2+} influx and the

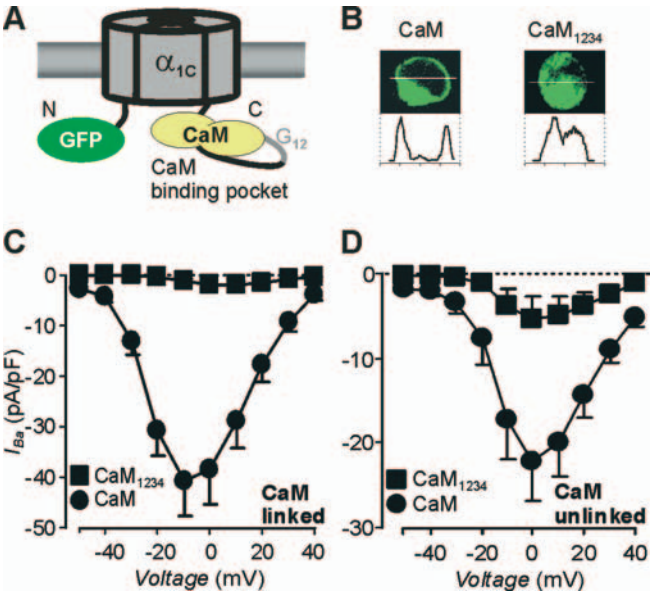

Figure 4. Trafficking of $Ca_V1.2$ channels to the plasma membrane is Ca^{2+}/CaM dependent. HEK293 cells stably expressing $\beta 1$ and $\alpha_2\delta$ were transfected with GFP-tagged α_{1C} linked to either CaM or CaM_{1234} (***A–C***) or with GFP-α_{1C} and additionally with CaM or CaM_{1234} separately (***D***). ***A***, Schematic of the CaM-linked GFP-tagged α_{1C} construct. ***B***, Representative confocal fluorescent images and accompanying line scans of cells expressing GFP–α_{1C}–CaM or GFP–α_{1C}–CaM_{1234}. ***C***, *I–V* relationships of I_{Ba} currents for cells expressing GFP–α_{1C}–CaM and GFP–α_{1C}–CaM_{1234} ($n = 7–11$). ***D***, *I–V* relationships of I_{Ba} currents for cells expressing GFP–α_{1C} and CaM or CaM_{1234} ($n = 7–11$).

consequent activation of gene expression cascades. Several activity-dependent gene expression pathways from synapse to nucleus have been dissected. In particular, activation of CREB has served as the quintessential model for this process (Deisseroth et al., 1996, 1998, 2003; West et al., 2002). Extensive investigation of the pathways leading to CREB activation in hippocampal neurons has revealed a privileged role for Ca^{2+} influx through $Ca_V1.2$ channels and the related $Ca_V1.3$ channels compared with other high voltage-activated (HVA) Ca^{2+} channels (e.g., $Ca_V2.1$ or $Ca_V2.2$) (Striessnig et al., 2006). Because the distinguishing feature among different HVA Ca^{2+} channels is the identity of the pore-forming α_1 subunit, the advantage of $Ca_V1.2$ and $Ca_V1.3$ channels must be attributable to specific determinants within the α_1 subunit rather than in the accessory β or $\alpha_2\delta$ subunits, which are common to all HVA channels (Ertel et al., 2000).

One key component affording $Ca_V1.2$ and $Ca_V1.3$ channels their privileged role in excitation–transcription coupling may therefore be the association between their respective α_1 subunits and CaM. Although CaM has also been predicted to interact with and confer Ca^{2+} sensitivity to gating of other HVA Ca^{2+} channels (Lee et al., 1999; DeMaria et al., 2001; Liang et al., 2003), the magnitude of the effect is markedly smaller, suggesting a different mode of interaction. An essential role for CaM interaction with α_{1C} ($Ca_V1.2$) in CREB-dependent gene expression was suggested by the disruption of excitation–transcription coupling when the CaM binding IQ motif in α_{1C} was mutated (Dolmetsch et al., 2001). Because CaM is but one CaBP that has been postulated to modulate Ca^{2+} channel function in neurons (Lee et al., 2002; Zhou et al., 2004; Lautermilch et al., 2005; Yang et al., 2006), our demonstration that CaM coimmunoprecipitates with α_{1C} from brain lysates provides the first evidence that CaM is a bona fide $Ca_V1.2$ subunit and the likely Ca^{2+} sensor for CDI and gene expression. Moreover, the recent demonstration that CaBP4 competes with CaM to modulate $Ca_V1.3$ channels in certain neuronal subpopulations (Yang et al., 2006) may explain the apparent differences in coupling of CREB activation to $Ca_V1.2$ versus $Ca_V1.3$ channels (Zhang et al., 2006).

The privileged role of $Ca_V1.2$ channels in excitation–transcription coupling may therefore derive from their specific manner of interaction with CaM. In its role as a channel subunit, CaM is positioned to contribute toward the Ca^{2+}-dependent regulation of any of the steps in channel biosynthesis that occur after subunit assembly. We found that CaM provides a Ca^{2+}-dependent acceleration of channel trafficking to distal regions of dendrites in hippocampal neurons. This adds to a growing list of examples in which CaM, as a constitutive subunit, modulates steps in channel biosynthesis such as trafficking of SK K^+ channels (Joiner et al., 2001; Lee et al., 2003) or assembly of KCNQ1 K^+ channels (Ghosh et al., 2006; Shamgar et al., 2006). For Ca^{2+}/CaM acceleration of α_{1C} trafficking, two results suggest that the mechanism of action for CaM most likely involves an interaction with the CaM binding pocket. First, we demonstrated that the CaM binding pocket contains a Ca^{2+}/CaM-dependent autonomous forward trafficking signal. This role for CaM and its binding pocket in α_{1C} trafficking/targeting fits well with the previous observation that a region in the α_{1C} CT, in which the CaM binding pocket resides, is important for membrane targeting (Gao et al., 2000). Second, mutations in the CaM binding pocket hindered α_{1C} trafficking. This latter result provides a possible explanation for the decreased gene expression seen with IQ motif mutations (Dolmetsch et al., 2001); these mutations possibly altered trafficking of α_{1C} to distal regions of the dendrites or reduced the amount of channels inserted into the membrane, thereby interfering with the gene expression cascade. In this context, it is interesting to note the previous report from Peterson et al. (1999), in which CaM_{1234} coexpression reduced peak $Ca_V1.2$ current amplitude in HEK cells compared with CaM coexpression. Because CaM_{1234} exerts its interference with CDI in a dominant-negative manner by precluding binding of CaM to the α_{1C} CaM binding pocket, the reduced current amplitude with CaM_{1234} coexpression recorded in that study, as in our results here, most likely arose from decreased trafficking/membrane insertion of α_{1C} subunits. Our quantification of gating charge and the visualization of the subcellular localization of GFP-tagged α_{1C} subunits here offer additional confirmation. As noted previously, it is important to consider that the specific manifestation of Ca^{2+}/CaM-mediated effects on channel trafficking/targeting in nonpolarized HEK cells may differ from that in neurons; nevertheless, the delayed trafficking in neurons and the reduced surface expression in HEK cells both appear to result from Ca^{2+}/CaM-mediated interaction with α_{1C}.

Because the mutations that disrupted CaM interaction markedly diminished both $Ca_V1.2$ current amplitude and affected trafficking, processes normally ascribed to Ca^{2+} channel β subunits (Dolphin, 2003), it is possible that CaM disruption impacts β subunit modulation. Consistent with this hypothesis, we demonstrated previously that the complex of α_{1C} CT and CaM could interact with the intracellular linker between the α_{1C} I–II domains (Kim et al., 2004), the primary sight for β subunit interaction. Moreover, the IQ motif contains the arginine- and lysine-rich sequence ^{1659}**RKFKKRK**^{1665}, a polybasic motif that could serve as an endoplasmic reticulum retention signal (Michelsen et al., 2005). Conserved among other HVA Ca^{2+} channels, the IQ motif may therefore contain the elusive α_1 ER retention signal, masked by CaM, that controls Ca^{2+} channel trafficking. The juxtaposition of CaM and the β subunit through the interaction

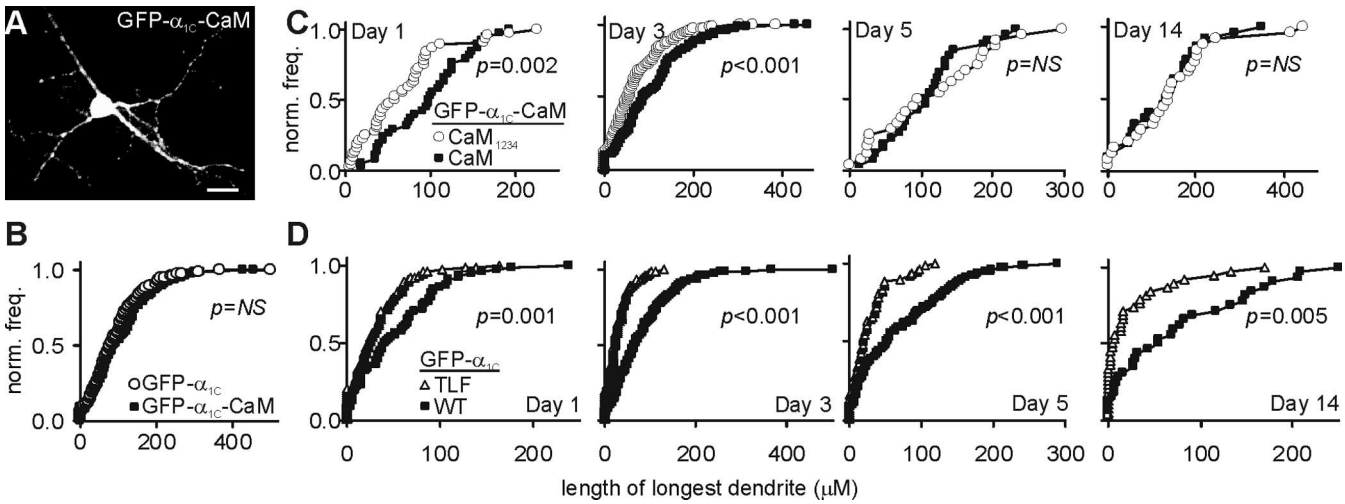

Figure 5. Trafficking of α_{1C} in hippocampal neurons is accelerated by Ca^{2+}/CaM. ***A***, Fluorescent confocal image of a hippocampal neuron transfected with GFP–α_{1C}–CaM. Scale bar, 20 μm. ***B***, Normalized frequency versus distance from soma of GFP in the longest dendrite for each neuron for GFP–α_{1C}–CaM ($n = 153$) or GFP–α_{1C} ($n = 193$) in cultures 3 d after transfection. ***C***, Normalized frequency versus distance from soma of GFP in the longest dendrite for each neuron for GFP–α_{1C}–CaM versus GFP–α_{1C}–CaM_{1234} in cultures imaged at day 1 (CaM, $n = 38$; CaM_{1234}, $n = 44$), day 3 (CaM, $n = 153$; CaM_{1234}, $n = 188$), day 5 (CaM, $n = 26$; CaM_{1234}, $n = 24$), and day 14 (CaM, $n = 22$; CaM_{1234}, $n = 25$) after transfection. ***D***, Same format as in ***C***. GFP–α_{1C} (WT) versus GFP–α_{1C} (TLF) for day 1 (WT, $n = 73$; TLF, $n = 111$), day 3 (WT, $n = 193$; TLF, $n = 130$), day 5 (WT, $n = 127$; TLF, $n = 180$), and day 14 (WT, $n = 32$; TLF, $n = 38$).

with the I–II linker could explain the contribution of β subunits to the trafficking process. In the specific case of α_{1C}, the dynamic regulation provided by CaM could be important in synaptic plasticity that depends on Ca^{2+} influx through $Ca_V1.2$ channels and is consistent with the data showing that Ca^{2+}/CaM interaction with the α_{1C} IQ motif contributes to activity-dependent gene expression (Dolmetsch et al., 2001).

In this regard, our observation that $Ca_V1.2$ channels were located in distal regions of dendrites, consistent with recent observations (Davare et al., 2001) that describe $Ca_V1.2$ channels in spines rather than an older report that suggested that $Ca_V1.2$ channels were restricted to the soma and proximal dendrites (Westenbroek et al., 1998), places $Ca_V1.2$ channels in the proper setting to initiate synapse to nucleus signaling. Ca^{2+}/CaM regulation of dendritic trafficking might therefore be an important component to the emerging model in which $Ca_V1.2$ channels participate in local signaling microdomains to regulate plasticity, even when the contribution of Ca^{2+} influx through the channels is modest. For example, long-term depression of synaptic activity depends on Ca^{2+} signaling through $Ca_V1.2$ channels and downstream activation of CaM kinase II in dendritic spines, yet Ca^{2+} influx through $Ca_V1.2$ channels is too small to be separated accurately from the dominant signal mediated by $Ca_v2.3$ (R-type) channels (Yasuda et al., 2003). Likewise, it is possible that CaM regulation of $Ca_V1.2$ trafficking may increase the local number of $Ca_V1.2$ channels in response to activity and participate in the specific role of $Ca_V1.2$ channels in NMDA receptor-independent plasticity and spatial memory (Moosmang et al., 2005). Such signaling pathways, possibly regulated by Ca^{2+}/CaM-mediated trafficking, may be vital for plasticity on the scale of individual synapses. Hence, determining the regulators of $Ca_V1.2$ localization in the dendritic arbor will prove to be important for our understanding of learning and memory.

References

Budde T, Meuth S, Pape HC (2002) Calcium-dependent inactivation of neuronal calcium channels. Nat Rev Neurosci 3:873–883.

Davare MA, Avdonin V, Hall DD, Peden EM, Burette A, Weinberg RJ, Horne MC, Hoshi T, Hell JW (2001) A beta 2 adrenergic receptor signaling complex assembled with the Ca^{2+} channel $Ca_v1.2$. Science 293:98–101.

Deisseroth K, Bito H, Tsien RW (1996) Signaling from synapse to nucleus: postsynaptic CREB phosphorylation during multiple forms of hippocampal synaptic plasticity. Neuron 16:89–101.

Deisseroth K, Heist EK, Tsien RW (1998) Translocation of calmodulin to the nucleus supports CREB phosphorylation in hippocampal neurons. Nature 392:198–202.

Deisseroth K, Mermelstein PG, Xia H, Tsien RW (2003) Signaling from synapse to nucleus: the logic behind the mechanisms. Curr Opin Neurobiol 13:354–365.

DeMaria CD, Soong TW, Alseikhan BA, Alvania RS, Yue DT (2001) Calmodulin bifurcates the local Ca^{2+} signal that modulates P/Q-type Ca^{2+} channels. Nature 411:484–489.

Deutsch C (2003) The birth of a channel. Neuron 40:265–276.

Dolmetsch RE, Pajvani U, Fife K, Spotts JM, Greenberg ME (2001) Signaling to the nucleus by an L-type calcium channel-calmodulin complex through the MAP kinase pathway. Science 294:333–339.

Dolphin AC (2003) b subunits of voltage-gated calcium channels. J Bioenerg Biomembr 35:599–620.

Ertel EA, Campbell KP, Harpold MM, Hofmann F, Mori Y, Perez-Reyes E, Schwartz A, Snutch TP, Tanabe T, Birnbaumer L, Tsien RW, Catterall WA (2000) Nomenclature of voltage-gated calcium channels. Neuron 25:533–535.

Gao T, Bunemann M, Gerhardstein BL, Ma H, Hosey MM (2000) Role of the C terminus of the alpha 1C (CaV1.2) subunit in membrane targeting of cardiac L-type calcium channels. J Biol Chem 275:25436–25444.

Ghosh S, Nunziato DA, Pitt GS (2006) KCNQ1 assembly and function is blocked by long-QT syndrome mutations that disrupt interaction with calmodulin. Circ Res 98:1048–1054.

Grabner M, Dirksen RT, Beam KG (1998) Tagging with green fluorescent protein reveals a distinct subcellular distribution of L-type and non-L-type Ca^{2+} channels expressed in dysgenic myotubes. Proc Natl Acad Sci USA 95:1903–1908.

Iodice L, Sarnataro S, Bonatti S (2001) The carboxyl-terminal valine is required for transport of glycoprotein CD8alpha from the endoplasmic reticulum to the intermediate compartment. J Biol Chem 276:28920–28926.

Joiner WJ, Khanna R, Schlichter LC, Kaczmarek LK (2001) Calmodulin regulates assembly and trafficking of SK4/IK1 Ca^{2+}-activated K^+ channels. J Biol Chem 276:37980–37985.

Kim J, Ghosh S, Nunziato DA, Pitt GS (2004) Identification of the components controlling inactivation of voltage-gated Ca^{2+} channels. Neuron 41:745–754.

Lautermilch NJ, Few AP, Scheuer T, Catterall WA (2005) Modulation of $Ca_V2.1$ channels by the neuronal calcium-binding protein visinin-like protein-2. J Neurosci 25:7062–7070.

Lee A, Wong ST, Gallagher D, Li B, Storm DR, Scheuer T, Catterall WA (1999) Ca^{2+}/calmodulin binds to and modulates P/Q-type calcium channels. Nature 399:155–159.

Lee A, Westenbroek RE, Haeseleer F, Palczewski K, Scheuer T, Catterall WA (2002) Differential modulation of Ca(v)2.1 channels by calmodulin and Ca^{2+}-binding protein 1. Nat Neurosci 5:210–217.

Lee WS, Ngo-Anh TJ, Bruening-Wright A, Maylie J, Adelman JP (2003) Small conductance Ca^{2+}-activated K^+ channels and calmodulin: cell surface expression and gating. J Biol Chem 278:25940–25946.

Liang H, DeMaria CD, Erickson MG, Mori MX, Alseikhan BA, Yue DT (2003) Unified mechanisms of Ca^{2+} regulation across the Ca^{2+} channel family. Neuron 39:951–960.

Michelsen K, Yuan H, Schwappach B (2005) Hide and run. Arginine-based endoplasmic-reticulum-sorting motifs in the assembly of heteromultimeric membrane proteins. EMBO Rep 6:717–722.

Moosmang S, Haider N, Klugbauer N, Adelsberger H, Langwieser N, Muller J, Stiess M, Marais E, Schulla V, Lacinova L, Goebbels S, Nave K-A, Storm DR, Hofmann F, Kleppisch T (2005) Role of hippocampal $Ca_v1.2$ Ca^{2+} channels in NMDA receptor-independent synaptic plasticity and spatial memory. J Neurosci 25:9883–9892.

Mori MX, Erickson MG, Yue DT (2004) Functional stoichiometry and local enrichment of calmodulin interacting with Ca^{2+} channels. Science 304:432–435.

Obermair GJ, Szabo Z, Bourinet E, Flucher BE (2004) Differential targeting of the L-type Ca^{2+} channel alpha 1C (CaV1.2) to synaptic and extrasynaptic compartments in hippocampal neurons. Eur J Neurosci 19:2109–2122.

Peterson BZ, DeMaria CD, Adelman JP, Yue DT (1999) Calmodulin is the Ca^{2+} sensor for Ca^{2+}-dependent inactivation of L-type calcium channels. Neuron [Erratum (1999) 22:893] 22:549–558.

Pitt GS, Zuhlke RD, Hudmon A, Schulman H, Reuter H, Tsien RW (2001) Molecular basis of calmodulin tethering and Ca^{2+}-dependent inactivation of L-type Ca^{2+} channels. J Biol Chem 276:30794–30802.

Shamgar L, Ma L, Schmitt N, Haitin Y, Peretz A, Wiener R, Hirsch J, Pongs O, Attali B (2006) Calmodulin is essential for cardiac IKS channel gating and assembly: impaired function in long-QT mutations. Circ Res 98:1055–1063.

Striessnig J, Koschak A, Sinnegger-Brauns MJ, Hetzenauer A, Nguyen NK, Busquet P, Pelster G, Singewald N (2006) Role of voltage-gated L-type Ca^{2+} channel isoforms for brain function. Biochem Soc Trans 34:903–909.

Weick JP, Groth RD, Isaksen AL, Mermelstein PG (2003) Interactions with PDZ proteins are required for L-type calcium channels to activate cAMP response element-binding protein-dependent gene expression. J Neurosci 23:3446–3456.

West AE, Griffith EC, Greenberg ME (2002) Regulation of transcription factors by neuronal activity. Nat Rev Neurosci 3:921–931.

Westenbroek RE, Hoskins L, Catterall WA (1998) Localization of Ca^{2+} channel subtypes on rat spinal motor neurons, interneurons, and nerve terminals. J Neurosci 18:6319–6330.

Yang PS, Alseikhan BA, Hiel H, Grant L, Mori MX, Yang W, Fuchs PA, Yue DT (2006) Switching of Ca^{2+}-dependent inactivation of $Ca_V1.3$ channels by calcium binding proteins of auditory hair cells. J Neurosci 26:10677–10689.

Yasuda R, Sabatini BL, Svoboda K (2003) Plasticity of calcium channels in dendritic spines. Nat Neurosci 6:948–955.

Zhang H, Fu Y, Altier C, Platzer J, Surmeier DJ, Bezprozvanny I (2006) Ca1.2 and CaV1.3 neuronal L-type calcium channels: differential targeting and signaling to pCREB. Eur J Neurosci 23:2297–2310.

Zhou H, Kim S-A, Kirk EA, Tippens AL, Sun H, Haeseleer F, Lee A (2004) Ca^{2+}-binding protein-1 facilitates and forms a postsynaptic complex with $Ca_v1.2$ (L-type) Ca^{2+} channels. J Neurosci 24:4698–4708.

Zühlke RD, Pitt GS, Deisseroth K, Tsien RW, Reuter H (1999) Calmodulin supports both inactivation and facilitation of L-type calcium channels. Nature 399:159–162.